Exploring the Role of the Nephelauxetic Effect in Circularly Polarized Luminescence of Chiral Chromium(III) Complexes

Poncet, Maxime Arnaud; Cuevas-Contreras, Laura; Ye, Yating; Guenee, Laure; Cruz, Carlos M; Piguet, Claude; Jiménez, Juan-Ramón

How to cite

PONCET, Maxime Arnaud et al. Exploring the Role of the Nephelauxetic Effect in Circularly Polarized Luminescence of Chiral Chromium(III) Complexes. In: Journal of the American Chemical Society, 2025, vol. 147, n° 27, p. 23827–23833. doi: 10.1021/jacs.5c06196

This publication URL: https://archive-ouverte.unige.ch/unige:186550
Publication DOI: 10.1021/jacs.5c06196

JACS
JOURNAL OF THE AMERICAN CHEMICAL SOCIETY
pubs.acs.org/JACS

Article

Exploring the Role of the Nephelauxetic Effect in Circularly Polarized Luminescence of Chiral Chromium(III) Complexes

Maxime Poncet, Laura Cuevas-Contreras, Yating Ye, Laure Guénée, Carlos M. Cruz, Claude Piguet,* and Juan-Ramón Jiménez*

Cite This: J. Am. Chem. Soc. 2025, 147, 23827−23833

Read Online

ACCESS | Metrics & More | Article Recommendations | Supporting Information

ABSTRACT: A novel chiral chromium(III) molecular ruby $[Cr(qpp)_2]^{3+}$ (qpp = *N*-methyl-*N*-(pyridin-2-yl)-6-(quinolin-8-yl)pyridin-2-amine) has been synthesized, enantiomerically resolved, and fully characterized. The circularly polarized luminescence (CPL) spectra revealed two emission bands of opposite polarization in the near-infrared region (700−800 nm), corresponding to the metal-centered transitions $Cr(^2T(1) \rightarrow {}^4A_2)$ and $Cr(^2E(1) \rightarrow {}^4A_2)$. Notably, the dissymmetry factor g_{lum} reached 0.11 for the former transition, which is among the highest reported for chromium(III) systems. Comparison with structurally related homo- and heteroleptic chromium(III) complexes underscores the important role of the nephelauxetic effect in tuning CPL properties. Increased metal−ligand covalency, indicative of a stronger nephelauxetic effect, enhances orbital mixing and modifies the electronic character of the emissive states. These changes influence both electric and magnetic transition dipole moments, leading to noticeable variations in dissymmetry factor g_{lum}. Altogether, these observations highlight the potential of fine-tuning metal−ligand covalency as a rational strategy for optimizing the chiroptical properties of chromium(III) complexes, with promising implications for bioimaging, molecular probes, and circularly polarized optoelectronic devices.

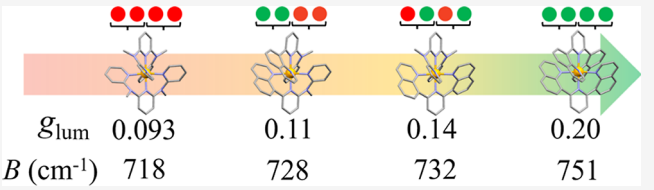

INTRODUCTION

Chiral chromium(III) complexes have garnered increasing interest as chiral luminophores due to their ability to exhibit a strong emission dissymmetry factor (g_{lum}) and circularly polarized luminescence (CPL) brightness (B_{CPL}).[1−4] These appealing properties make them promising candidates for applications in bioimaging, light-emitting devices, and molecular probes.[5−8] The sharp light emissions arising from the low-lying excited states $Cr(^2E,{}^2T_1 \rightarrow {}^4A_2)$, so-called "spin-flip" transitions (SF), display long excited state lifetimes accompanied by high photoluminescence quantum yields (Φ_{PL}) when strong field tridentate six-membered chelate ring ligands are coordinated to the metal center.[9,10] As a result of the chemical inertness of chromium(III), stable configuration and chirality can arise from the formation of the chelate rings with the helically twisted C_2-symmetrical ditridentate ligands dqp and ddpd in $[Cr(\mathbf{L})_2]^{3+}$ complexes (**L** = dqp = 2,6-di(quinolin-8-yl)pyridine, **L** = ddpd = N^2,N^6-dimethyl-N^2,N^6-di(pyridin-2-yl)pyridine-2,6-diamine; Figure 1a,d).[11−13] The SF transitions in chromium(III) complexes, which consist in the rearrangement of the electrons within the $t_2(\pi)$ orbitals, are forbidden by both the spin and Laporte selection rule, leading to comparable magnitudes for the electric (μ) and magnetic (m) transition dipole moments.[14,15] This is crucial for enhancing the dissymmetry factor (g_{lum}), which represents the degree of "enantiorichness" of the CPL emitted by a chiral luminophore at a given wavelength (eq. 1). Moreover, to maximize the g_{lum}, these two vectors should be collinear (θ = 0° or 180°).[1,16]

$$|g_{lum}| = 4 \times \frac{(\mu/m) \times \cos\ \theta}{(\mu/m)^2 + 1} \quad (1)$$

Since the energies of SF states in this type of compounds are largely independent of the ligand-field splitting (Δ_{oct}), increasing metal−ligand covalency through the nephelauxetic effect presents a viable strategy for shifting these states to lower energies.[17−23] However, this approach comes at a cost as the enhanced covalency leads to increased mixing or "cloud-expanding" of the metal−ligand orbitals, resulting in a loss of their pure SF character and thus the modification of the transition dipole moments of the transition. This, in turn, can impact the magnitude of g_{lum}.[24−26] In this work, we investigate how subtle variations in the metal−ligand covalency (nephelauxetic effect) affect the magnitude of g_{lum} in a series of structurally related chiral chromium(III) complexes (Figure 1).

Received: April 11, 2025
Revised: June 17, 2025
Accepted: June 18, 2025
Published: June 28, 2025

https://doi.org/10.1021/jacs.5c06196
J. Am. Chem. Soc. 2025, 147, 23827−23833

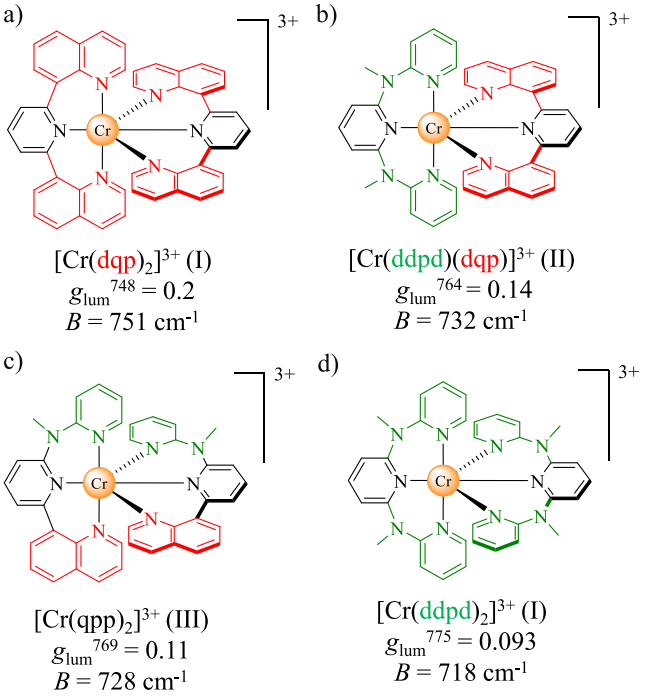

Figure 1. Molecular structures of (a) [Cr(dqp)$_2$]$^{3+}$, (b) [Cr(dqp)(ddpd)]$^{3+}$, (c) [Cr(qpp)$_2$]$^{3+}$, and (d) [Cr(ddpd)$_2$]$^{3+}$ with their respective g_{lum} and Racah parameter *B*.

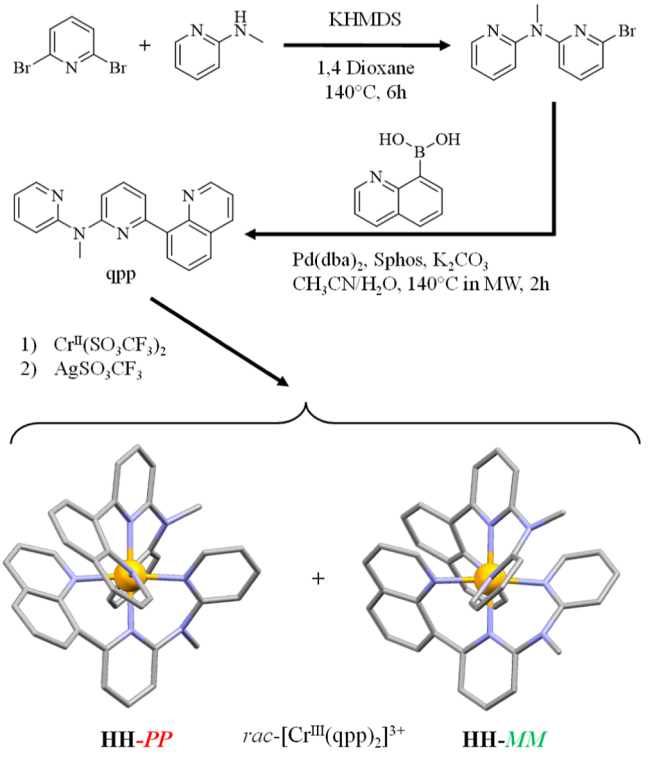

Figure 2. Synthesis of the organic ligand qpp and synthesis of the homoleptic complex *rac*-HH-[Cr(qpp)$_2$](SO$_3$CF$_3$)$_3$.

RESULTS AND DISCUSSION

Synthesis and Structural Properties. As a starting point, let us consider the previously studied helically chiral homoleptic *PP*/*MM*-[Cr(dqp)$_2$]$^{3+}$ and *PP*/*MM*-[Cr(ddpd)$_2$]$^{3+}$ (D_2-symmetry, structure I in Scheme S1) and heteroleptic *PP*/*MM*-[Cr(dqp)(ddpd)]$^{3+}$ (C_2-symmetry, structure II in Scheme S1) compounds, the dissymmetry factors of which reach $|g_{lum}^{748}| = 0.20$, $|g_{lum}^{775}| = 0.093$ and $|g_{lum}^{764}| = 0.14$, respectively, for the lower energy SF transition (Figure 1a,b,d).[4,13,27] The alternative side-by-side nonchiral *PM* isomers are destabilized by the lack of interstrand packing interactions and were never observed. They are therefore not considered further in this work. For exploring chirality beyond symmetrical double-helical arrangement in these systems, a new inert chromium complex [Cr(qpp)$_2$]$^{3+}$ has been prepared using the dissymmetric ligand qpp (qpp = *N*-methyl-*N*-(pyridin-2-yl)-6-(quinolin-8-yl)pyridin-2-amine, Figure 2 and Supporting Information for synthetic details) which corresponds to a "half-dqp/half-ddpd" tridentate binding unit containing a central pyridine flanked with a quinoline and a *N*-methylpyridin-2-amine terminal groups (Figure 1c). The homoleptic complex *rac*-[Cr(qpp)$_2$]$^{3+}$ could be synthesized by reaction with labile Cr^{II}(SO$_3$CF$_3$)$_2$ followed by oxidation with AgSO$_3$CF$_3$ to yield air-stable inert *rac*-[Cr(qpp)$_2$]$^{3+}$ (Figure 2 and Supporting Information for synthetic details).

Slow diffusion of diethyl ether in a concentrated solution of methanol yielded X-ray-quality crystals, showing the exclusive formation of a racemic mixture of the head-to-head HH-*PP*/*MM* [Cr(qpp)$_2$]$^{3+}$ diastereomer (C_2-symmetry, structure III in Scheme S1) where both ligands are meridionally wrapped around the metallic center (Figures 2 and S1 and Tables S1 and S2, CCDC-2428511), thus allowing the operation of stabilizing interstrand homotopic quinoline/quinoline interactions (interplanar angles of 15.53°, Figures 2 and S2 and S3).

The transoid bite angles N−Cr−N are in the 173.76(14)°−178.71(16)° range, in line with only minor distortions from perfect octahedron ascertained by (i) $\Sigma = \sum_{i=1}^{12}|90 - \varphi_i| = 31.97°$ (φ_i are the cisoid bite angles N−Cr−N) similar to those reported for heteroleptic [Cr(dqp)(ddpd)]$^{3+}$ and homoleptic [Cr(dqp)$_2$]$^{3+}$ and [Cr(ddpd)$_2$]$^{3+}$ parent complexes (28.9° to 37.1°, Figure S2) and (ii) continuous shape measurements (CShMs,[28] Table S3). Thus, all four compounds exhibit essentially identical geometrical characteristics, both in their primary coordination spheres and in their ligand distortions. However, one notes that the average Cr−N bond distance in the "full-terminal quinoline" [Cr(dqp)$_2$]$^{3+}$ complex (2.060(3) Å) is longer than those observed in all complexes containing terminal pyridine ligands in [Cr(ddpd)$_2$]$^{3+}$ (2.044(5) Å), [Cr(dqp)(ddpd)]$^{3+}$ (2.045(5) Å) and [Cr(qpp)$_2$]$^{3+}$ (2.047(3) Å, Figure S2), which suggests variable covalent characters and different nephelauxetic effect (vide infra).

Absorption and Emission Properties. The absorption spectrum of the novel HH-*rac*-[Cr(qpp)$_2$]$^{3+}$compound was recorded at room temperature in acetonitrile at different concentrations to observe all of the active transitions of the complex (Figures 3 and S4 and Table S4). The 250−350 nm region (40,000−28,571 cm^{-1}) is dominated by intense allowed ligand-centered $\pi^* \leftarrow \pi$ transitions. Charge transfers (CTs) transitions are located in the visible range 350−500 nm (28,571−20,000 cm^{-1}) while the shoulder located at 420−440 nm (23,810−22,727 cm^{-1}) has been tentatively assigned to the spin-allowed metal-centered (MC) transition Cr($^4T_2 \leftarrow {}^4A_2$) according to TD-DFT calculations (Tables S8 and S10 and Figures S16, S19, S21 and S22). Because of the d^3 electronic configuration in the octahedral geometry, this transition is a direct measure of the ligand field splitting energy Δ_{oct}. Similar values of Δ_{oct} are found within the family (Table 1, column 4). At lower energy, the weak doubly forbidden SF transitions

https://doi.org/10.1021/jacs.5c06196
J. Am. Chem. Soc. 2025, 147, 23827−23833

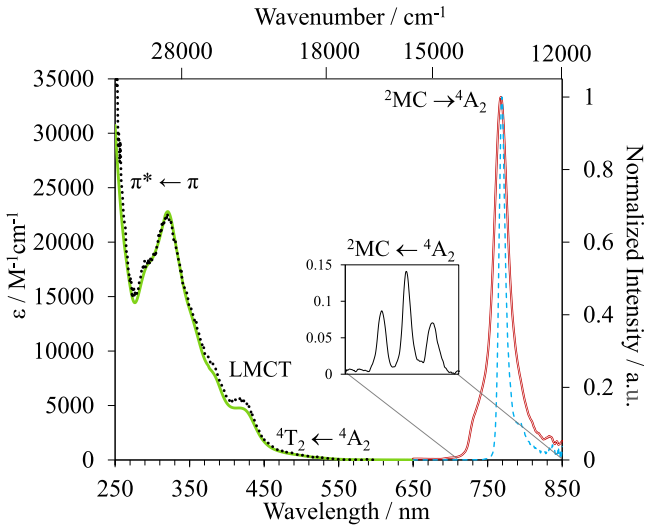

Figure 3. Absorption spectra (green trace), excitation spectrum (λ_{em} = 769 nm, dashed black trace), emission spectrum at room temperature (λ_{exc} = 400 nm, red trace), and emission spectrum at 77 K (λ_{exc} = 400 nm, dashed blue trace) of $[Cr(qpp)_2]^{3+}$ in CH_3CN at 3.3×10^{-5} M.

$Cr(^2T_1,^2E \leftarrow {}^4A_2)$ are observed within the 680−800 nm (14,706−12,500 cm^{-1}) range with ε reaching 0.14 M^{-1} cm^{-1} (Figures 3 inset and S4 and Table S4). The (very) minor splitting of the chromium(III)-based spin-flip transitions supports (Figures 3 and S18) the use of octahedral irreducible labels ($^4A_2$, ^2E, $^2T_1$, and $^4T_2$) for characterizing the intrashell d−d transitions.

Upon UV−vis excitation, HH-*rac*-$[Cr(qpp)_2]^{3+}$ displays a sharp near-infrared (NIR) dual emission band with a maximum at 769 nm (13,003 cm^{-1}) and a shoulder at 730 nm (13,698 cm^{-1}). Similar dual SF emissions are observed within the complete family of chromium complexes with varying intensity ratios depending on the energy difference between these thermally equilibrated states (Figure S5). The excited state landscape was evaluated using the complete active space self-consistent field method (CASSCF(7,12)/FIC-NEVPT2) for the four complexes. The calculations revealed a similar distribution of the excited states in the four compounds, where the microstates $^2T_1(1)$ and $^2E(1)$, derived from the lowering symmetry ($O \rightarrow D_2$), are the lowest energy excited states (Table S7 and Figure S18). Therefore, the dual emission originates from the $Cr(^2T(1) \rightarrow {}^4A_2)$ and Cr ($^2E(1) \rightarrow {}^4A_2$) transitions according to theoretical calculations, with the latter corresponding to the higher-energy one (Figures 3 and S18 and Table S7).

Finally, the associated excitation spectrum of HH-$[Cr(qpp)_2]^{3+}$ closely matches its absorption spectrum (Figure 3), thus making this complex a good candidate for UV to NIR light-downshifting.

Beyond minor specific second-order corrections $\alpha B^2/\Delta_{oct}$, the energy of both excited $Cr(^2T_1)$ and $Cr(^2E)$ levels is mainly separated by $9B + 3C$ from the ground state $Cr(^4A_2)$ in pure octahedral complexes (B and C are the Racah parameters).[29] Accordingly, the systematic red-shifts of the $Cr(^2T(1) \rightarrow {}^4A_2)$ and $Cr(^2E(1) \rightarrow {}^4A_2)$ transition observed along the series $[Cr(ddpd)_2]^{3+}$ > $[Cr(qpp)_2]^{3+}$ ≈ $[Cr(dqp)(ddpd)]^{3+}$ > $[Cr(dqp)_2]^{3+}$ (Table 1, columns 2 and 3 and Figure S5) suggest the operation of increasing nephelauxetic effect and larger electron delocalization which, as a first approximation, can be inferred from the decreasing value of the Racah parameter B (Table 1, column 5).[22,23] It is important noticing that the $Cr(^2T(1) \rightarrow {}^4A_2)$ emission displays a more pronounced red-shift compared to the $Cr(^2E(1) \rightarrow {}^4A_2)$, indicating that the former transition is more influenced by changes in metal−ligand interactions (Figure S5). This difference has been attributed by Heinze and co-workers to the greater ability of the two paired electrons in the $^2T(1)$ state to delocalize through the ligand.[30,31]

Due to the weak distortion and strong ligand-field splitting, nonradiative deexcitation pathways are prevented and the Φ_{PL} reaches 8% in the absence of $^3O_2$, which is in the range of the highest reported deuterium-free Cr^{III} molecular complexes (Table 2) with excited state lifetimes of $\tau_{Cr,obs}^{^2E',^2T_1'}$ = 1.41 ms at 77 K (Figure S6) and 422 μs at 298 K (Figures S7 and S8). Under air-equilibrated conditions, the Φ_{PL} drops to 0.4% and $\tau_{Cr,obs}^{^2E',^2T_1'}$ = 33 μs due to the presence of $^3O_2$ in solution (Figures S9). The radiative rate for the low energy ^2MC excited state, k_{rad}, has been estimated assuming that the intersystem crossing between the ^4MC and ^2MC states is close to unity (i.e., $k_{rad} = \Phi/\tau_{obs}$).[32] The computed values for $[Cr(dqp)_2]^{3+}$ (87 s^{-1}) < $[Cr(dqp)(ddpd)]^{3+}$ (93 s^{-1}) < $[Cr(qpp)_2]^{3+}$ (121 s^{-1}) < $[Cr(ddpd)_2]^{3+}$ (125 s^{-1}) have been calculated in deaerated solutions for reliability (Table S12).[12,20] Importantly, larger k_{rad} values are associated with less restricted spin-forbidden transitions and greater covalency.

Chiral Resolution, Circular Dichroism, and Circularly Polarized Luminescence. Enantiomeric resolution of the racemic mixture HH-*rac*-$[Cr(qpp)_2]^{3+}$ was achieved by using chiral stationary phase HPLC (CSP HPLC; Figure S10). Subsequent circular dichroism (CD) and circularly polarized luminescence (CPL) measurements were successfully carried out for both enantiomers (Figure 4a,b). Mirror images are consistently obtained in both CD and CPL experiments. The

Table 1. Photophysical and Chiroptical Parameters

complex	λ_{em}[a] (nm) $^2E(1) \rightarrow {}^4A_2$	λ_{em}[a] (nm) $^2T_1(1) \rightarrow {}^4A_2$	Δ_{oct}[b] (cm^{-1})	B[c] (cm^{-1}) C/B = 3.2/C/B = 4	β[d]	$\lvert g_{lum}\rvert$[e] $^2T_1 \rightarrow {}^4A_2$	$\lvert g_{lum}\rvert$[e] $^2E \rightarrow {}^4A_2$
$[Cr(dqp)_2]^{3+}$	725	748	22,969	751:659	0.79	0.2	0.1
$[Cr(dqp)(ddpd)]^{3+}$	729	764	23,353	732:642	0.77	0.14	0.07
$[Cr(qpp)_2]^{3+}$	729	769	23,283	728:639	0.76	0.11	0.08
$[Cr(ddpd)_2]^{3+}$	733	775	23,626	718:630	0.75	0.093	0.06

[a]λ_{em} from emission spectra at 293 K. [b]Δ_{oct} extracted from CASSCF(7,12)/FIC-NEVPT2 (Table S7). [c]Racah parameter B assuming a fixed C/B ratio, $E(^4T_2) = \Delta_{oct}$, and $E(^2T_1) = 9B + 3C - 24(B^2/\Delta_{oct})$.[29] The $E(^2T_1)$ state has been extracted from the emission spectrum at 77 K (Figure S5). [d]Nephelauxetic parameter β (B/B_0) where B_0 is 950 cm^{-1} for free Cr^{III} ion in the gas phase.[17] [e]Dissymmetry factor g_{lum} was determined at the emission band maximum.

https://doi.org/10.1021/jacs.5c06196
J. Am. Chem. Soc. 2025, 147, 23827−23833

Table 2. CPL Brightness (B_{CPL}) Calculation for Each Emissive Transitions in Selected Di-tridentate Chromium Complexes

complex	ε/M^{-1} cm^{-1}	ϕ_{PL}/%[d]	$^2T_1'/^2E'$ ratio		$\lvert g_{lum}\rvert$	B_{CPL}/M^{-1} cm^{-1}
$[Cr(dqp)_2]^{3+}$	20,000[a]	10.4	$^2E'$	0.315	0.1	33
			$^2T_1'$	0.685	0.2	142
$[Cr(ddpd)_2]^{3+}$	30,000[b]	12.1	$^2E'$	0.136	0.06	13
			$^2T_1'$	0.864	0.093	146
$[Cr(dqp)(ddpd)]^{3+}$	32,684[c]	6.0	$^2E'$	0.181	0.07	14
			$^2T_1'$	0.819	0.14	112
$[Cr(qpp)_2]^{3+}$	16,547[c]	8.0	$^2E'$	0.072	0.08	4
			$^2T_1'$	0.928	0.11	68

[a]λ_{abs} = 370 nm. [b]λ_{abs} = 405 nm. [c]λ_{abs} = 340 nm. [d]Deaerated conditions.

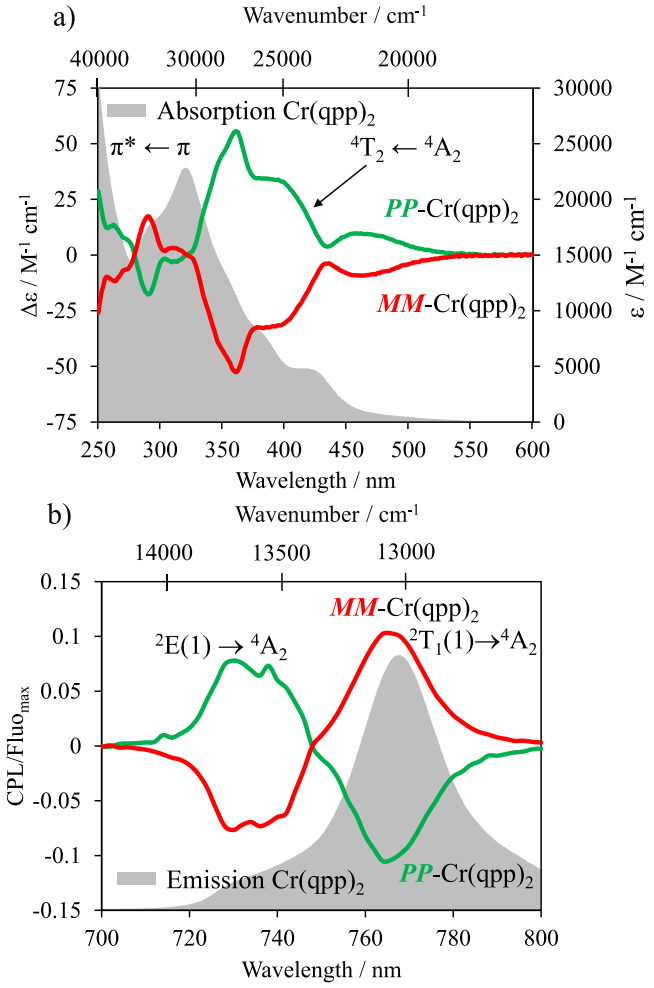

Figure 4. (a) CD spectra of both enantiomers HH-*PP*-$[Cr(qpp)_2]^{3+}$ (green trace) and HH-*MM*-$[Cr(qpp)_2]^{3+}$ (red trace) and corresponding absorption spectra (gray surface). (b) CPL spectra of both enantiomers HH-*PP*-$[Cr(qpp)_2]^{3+}$ (green trace) and HH-*MM*-$[Cr(qpp)_2]^{3+}$ (red trace) and corresponding emission spectra (gray surface). Recorded in EtOH/CH_2Cl_2 (1:1) at 293 K.

assignment to the *PP* and *MM* configurations was made possible by comparing their CD spectra with that of the analogue pure *MM*-$[Cr(dqp)_2]^{3+}$ enantiomer, which could be crystallized.[13] This assignment is further confirmed by theoretical calculations (Figure S20).

In the CD spectrum, a strong Cotton effect is observed within the 330−430 nm range reaching up to $|\Delta\varepsilon|$ = 55.6 M^{-1} cm^{-1} (Table S5), which can be attributed to the MC Cr($^4T_2$ ← $^4A_2$) transition (Figure 4a). CPL measurements were recorded with an experimental bandwidth (EBW) of 2.4 nm to ensure a high resolution.[24] Under unpolarized excitation (λ_{exc} = 350 nm), HH-*PP*/*MM*-$[Cr(qpp)_2]^{3+}$ enantiomers display dual and strong circularly polarized emission in the NIR region (Figure 4b) with $|g_{lum}|$ = 0.11 for the Cr($^2T_1(1) \rightarrow {}^4A_2$) transition at 769 nm and 0.08 at 730 nm for Cr ($^2E(1) \rightarrow {}^4A_2$) (Figure S11). The CPL of the compounds *PP*/*MM*-$[Cr(dqp)_2]^{3+}$ and *PP*/*MM*-$[Cr(dqp)(ddpd)]^{3+}$ have been already measured by our group,[4,13] whereas *PP*/*MM*-$[Cr(ddpd)_2]^{3+}$ reported by Dee et al.[27] has been re-evaluated in this work under identical experimental conditions to ensure consistency within the family of compounds. We found a dual CPL emission with $|g_{lum}|$ = 0.094 for the Cr($^2T_1(1) \rightarrow {}^4A_2$) and 0.06 for Cr($^2E(1) \rightarrow {}^4A_2$) transitions (Figure S12).

While they are of the same order of magnitude, subtle differences can be observed for the $|g_{lum}|$ values of the two transitions in all four chromium complexes (Table 1, columns 7 and 8). First, the isoelectronic $[Cr(dqp)(ddpd)]^{3+}$ and $[Cr(qpp)_2]^{3+}$ complexes display appreciable different CPL responses that might be related to different geometrical constraints resulting from the nature of the interstrand stacking interactions which are of homoleptic type in HH-$[Cr(qpp)_2]^{3+}$ (quinoline−quinoline and pyridine−pyridine) and of heteroleptic type in $[Cr(dqp)(ddpd)]^{3+}$ (twice quinoline−pyridine, Figures S2 and S3). Second, the estimated g_{lum} values for the Cr($^2T_1(1) \rightarrow {}^4A_2$) and Cr($^2E(1) \rightarrow {}^4A_2$) transitions within this family of complexes decrease as the SF emission undergoes a bathochromic shift (i.e., red-shift). This trend suggests a possible relationship between g_{lum} and the nephelauxetic effect which reflects metal-to-ligand electron delocalization.[33] To explore this proposal, the Racah parameters *B* and *C*, taken as probes for the metal−ligand covalency and electronic delocalization, have been calculated assuming the relationships *C*/*B* = 3.2 and *C*/*B* = 4.[29,34,35] (Table 1, column 5).[29,33] Assuming a fixed *C*/*B* ratio simplifies the ligand-field analysis. However, detailed and systematic ligand-field studies of the electronic spectra of Cr^{III} compounds—and more recently Co^{III} complexes—have shown that *C*/*B* values can vary considerably, typically ranging from 3 to 10.[36,37] Our primary focus of our work is on the correlation between the estimated *B* parameters and the experimental g_{lum} values. We believe that even though the absolute values of *B* may be affected by the chosen *C*/*B* ratio, the relative trends across the series are more robust, assuming that a consistent approach is applied throughout. The decrease of *B* along $[Cr(dqp)_2]^{3+}$ (751 cm^{-1}) > $[Cr(dqp)(ddpd)]^{3+}$ (732 cm^{-1}) ≈ $[Cr(qpp)_2]^{3+}$ (728 cm^{-1}) > $[Cr(ddpd)_2]^{3+}$ (718 cm^{-1}) implies some stepwise increase of metal−ligand covalency and electron delocalization upon replacement of terminal quinoline with *N*-methyl

https://doi.org/10.1021/jacs.5c06196
J. Am. Chem. Soc. 2025, 147, 23827−23833

pyridine-2-amine units (Table 1), a trend confirmed by Ab Initio Ligand Field parameters computed from CASSCF(3,5)/FIC-NEVPT2 (Table S6). The nephelauxetic effect is often quantified by the nephelauxetic parameter (β), which is the ratio between the Racah B parameter of a given ion in the gas phase (B_0).[17] For the reported compounds β ranges between 0.79 and 0.75 in going from $[Cr(dqp)_2]^{3+}$to $[Cr(ddpd)_2]^{3+}$ (Table 1 column 6). The concomitant decrease in g_{lum} (from 0.2 to 0.093) highlights the impact of the nephelauxetic effect on the chiroptical response of these complexes. The expanded delocalization of d-electrons due to a larger nephelauxetic effect (small B and β values) is expected to enhance mixing of the metal-ligand orbitals, thus partially relaxing the doubly forbidden character of the SF transition, further increasing the electric dipole transition moments (μ). Since g_{lum} is maximized when the electric dipole transition moment is minimized to become comparable with magnetic dipole transition moments (eq 1),[2] its slight increase with nephelauxetic effect (covalency) should result in a decrease of the g_{lum} response (Table 1). To support this hypothesis, recent homoleptic pseudo-octahedral Cr^{III} complexes containing anionic tridentate 1,8-(bisoxazolyl)carbazolide ligands and displaying very large nephelauxetic effect with $Cr(^2T_1,^2E \rightarrow {}^4A_2)$ phosphorescence in the range of 813−845 nm have been shown to induce circularly polarized NIR emissions with unusually small g_{lum} in the scale of 2.0×10^{-3}.[38] Furthermore, Hasegawa and co-workers showed that the mixing of LMCT configurations into f−f excited states can perturb the electric and magnetic transition dipole moments, thereby affecting the CPL properties of chiral Eu^{III} complexes.[39,40]

Finally, B_{CPL}, calculated as $B_{CPL} = \varepsilon \times \phi_{PL} \times 1/2 \times |g_{lum}|$, is estimated for each transition (Table 2). Because g_{lum} is of opposite signs for $Cr(^2T_1(1) \rightarrow {}^4A_2)$ and $Cr(^2E(1) \rightarrow {}^4A_2)$ transitions (Figure 4b), a spectral deconvolution was necessary to accurately extract individual contributions to B_{CPL} (Figures S13−S15). This step is essential because the observed total emission (Figure S5) is a convolution of these two transitions, each contributing with different ϕ_{PL} and g_{lum}. By resolving each transition's spectral profile ($^2T_1'/^2E'$ ratio in Table 2), we could accurately integrate the individual emission bands, determine their respective quantum yields, and subsequently calculate the corrected B_{CPL} values (Table 2). This deconvolution approach ensures a more reliable assessment of B_{CPL}, avoiding misleading estimations due to spectral overlap and sign cancellation effects in g_{lum}. Respectable values of B_{CPL} have been extracted for the new analogue $[Cr(qpp)_2]^{3+}$ (Table 2, column 6) being some order of magnitude larger that most chiral organic molecules and chiral 4d and 5d-based metal complexes.[2]

CONCLUSION

In conclusion, an up-to-now not recognized consequence of the nephelauxetic effect on the chiroptical properties of chromium(III) complexes is suggested, with a particular focus on their g_{lum} and CPL behavior. Modulating metal−ligand covalency, particularly through ligand design, may influence the electronic structure and the magnitude of the transition dipole moments (μ and m). This plays a crucial role in the rational modulation of g_{lum} as it directly impacts the efficiency and alignment of chiroptical transitions. The red-shifted spin-forbidden emission controlled by the modulation of the nephelauxetic effect (i.e., the decrease of Racah B parameter) suggests that increased covalent character in the metal−ligand bond favors orbital mixing and decreases the g_{lum} factor. These findings offer new avenues for optimizing CPL properties in chromium(III) complexes, distinguishing them from benchmark europium(III) complexes by providing systems with improved luminescence efficiency without sacrificing the g_{lum} value.[41] However, due to the limited number of examples in the literature, further studies involving a broader range of chromium(III)-based complexes are necessary to fully explore the implications of this hypothesis.

ASSOCIATED CONTENT

Supporting Information

The Supporting Information is available free of charge at https://pubs.acs.org/doi/10.1021/jacs.5c06196.

Experimental details; theoretical calculations; list of transition bands; and decay curves (PDF)

Accession Codes

Deposition number 2428511 contains the supplementary crystallographic data for this paper. These data can be obtained free of charge via the joint Cambridge Crystallographic Data Centre (CCDC) and Fachinformationszentrum Karlsruhe Access Structures service.

AUTHOR INFORMATION

Corresponding Authors

Claude Piguet − *Department of Inorganic and Analytical Chemistry, University of Geneva, CH-1211 Geneva, Switzerland;* orcid.org/0000-0001-7064-8548; Email: Claude.Piguet@unige.ch

Juan-Ramón Jiménez − *Departamento de Química Inorgánica, Facultad de Ciencias, Unidad de Excelencia de Química Aplicada a Biomedicina y Medioambiente, 18071 Granada, Spain;* orcid.org/0000-0003-3871-3594; Email: jrjimenez@ugr.es

Authors

Maxime Poncet − *Department of Inorganic and Analytical Chemistry, University of Geneva, CH-1211 Geneva, Switzerland;* orcid.org/0000-0001-8649-7991

Laura Cuevas-Contreras − *Departamento de Química Inorgánica, Facultad de Ciencias, Unidad de Excelencia de Química Aplicada a Biomedicina y Medioambiente, 18071 Granada, Spain*

Yating Ye − *Departamento de Química Inorgánica, Facultad de Ciencias, Unidad de Excelencia de Química Aplicada a Biomedicina y Medioambiente, 18071 Granada, Spain;* orcid.org/0000-0002-1003-4285

Laure Guénée − *Laboratory of Crystallography, University of Geneva, CH-1211 Geneva, Switzerland*

Carlos M. Cruz − *Departamento de Química Orgánica, Facultad de Ciencias, Unidad de Excelencia de Química Aplicada a Biomedicina y Medioambiente, 18071 Granada, Spain;* orcid.org/0000-0002-0676-5210

Complete contact information is available at: https://pubs.acs.org/10.1021/jacs.5c06196

Author Contributions

The manuscript was written through contributions of all authors. All authors have given approval to the final version of the manuscript.

Notes

The authors declare no competing financial interest.

■ ACKNOWLEDGMENTS

Financial support from the Swiss National Science Foundation is gratefully acknowledged (grant 200020_207313). The funding received from the grant TED2021.129598A.I00 funded by MCIN/AEI/10.13039/501100011033 and by European Union NextGenerationEU/PRTR and to the Ministerio de Ciencia Innovación y Universidades for a Ramón y Cajal contract (grant RYC2022-037255-I) funded by MCIN/AEI/10.13039/501100011033 and ESF+ is also gratefully acknowledged. C.M.C. acknowledges grant PID2022-137403NA-I00 funded by MICIU/AEI/10.13039/501100011033 and by ERDF/EU, and grant RYC2023-044652-I funded by MICIU/AEI/10.13039/501100011033 and by ESF+.

■ REFERENCES

(1) Jiménez, J.-R.; Poncet, M.; Miguez-Lago, S.; Grass, S.; Lacour, J.; Besnard, C.; Cuerva, J. M.; Campaña, A. G.; Piguet, C. Bright Long-Lived Circularly Polarized Luminescence in Chiral Chromium (III) Complexes. *Angew. Chem., Int. Ed.* **2021**, *60*, 10095−10102.

(2) Arrico, L.; Di Bari, L.; Zinna, F. Quantifying the Overall Efficiency of Circularly Polarized Emitters. *Chem. - Eur. J.* **2021**, *27*, 2920−2934.

(3) Willis, O. G.; Zinna, F.; Di Bari, L. NIR-Circularly Polarized Luminescence from Chiral Complexes of Lanthanides and d-Metals. *Angew. Chem., Int. Ed.* **2023**, *62* (25), 1−11.

(4) Poncet, M.; Besnard, C.; Guénée, L.; Jiménez, J.-R.; Piguet, C. Tuning the Circularly Polarized Luminescence in Homoleptic and Heteroleptic Chiral CrIII Complexes. *Front. Chem.* **2024**, *12* (October), 1472943.

(5) Liang, N.; Cao, C.; Xie, Z.; Liu, J.; Feng, Y.; Yao, C. J. Advances in Near-Infrared Circularly Polarized Luminescence with Organometallic and Small Organic Molecules. *Mater. Today* **2024**, *75*, 309−333.

(6) Zinna, F.; Di Bari, L. Lanthanide Circularly Polarized Luminescence: Bases and Applications. *Chirality* **2015**, *27*, 1−13.

(7) Furlan, F.; Moreno-Naranjo, J. M.; Gasparini, N.; Feldmann, S.; Wade, J.; Fuchter, M. J. Chiral Materials and Mechanisms for Circularly Polarised Light-Emitting Diodes. *Nat. Photonics* **2024**, *18*, 658−668.

(8) Mackenzie, L. E.; Pal, R. Circularly Polarized Lanthanide Luminescence for Advanced Security Inks. *Nat. Rev. Chem.* **2021**, *5*, 109−124.

(9) Otto, S.; Dorn, M.; Förster, C.; Bauer, M.; Seitz, M.; Heinze, K. Understanding and Exploiting Long-Lived near-Infrared Emission of a Molecular Ruby. *Coord. Chem. Rev.* **2018**, *359*, 102−111.

(10) Kitzmann, W. R.; Moll, J.; Heinze, K. Spin-Flip Luminescence. In *Photochemical and Photobiological Sciences*; Springer International Publishing, 2022; pp 1309−1331.

(11) Jiménez, J. R.; Doistau, B.; Poncet, M.; Piguet, C. Heteroleptic Trivalent Chromium in Coordination Chemistry: Novel Building Blocks for Addressing Old Challenges in Multimetallic Luminescent Complexes. *Coord. Chem. Rev.* **2021**, *434*, 213750.

(12) Otto, S.; Grabolle, M.; Förster, C.; Kreitner, C.; Resch-Genger, U.; Heinze, K. [Cr(ddpd)2]3+: A Molecular, Water-Soluble, Highly NIR-Emissive Ruby Analogue. *Angew. Chem., Int. Ed.* **2015**, *54* (39), 11572−11576.

(13) Jiménez, J. R.; Doistau, B.; Cruz, C. M.; Besnard, C.; Cuerva, J. M.; Campaña, A. G.; Piguet, C. Chiral Molecular Ruby [Cr(dqp)2]3+ with Long-Lived Circularly Polarized Luminescence. *J. Am. Chem. Soc.* **2019**, *141* (33), 13244−13252.

(14) Doistau, B.; Jiménez, J. R.; Piguet, C. Beyond Chiral Organic (p-Block) Chromophores for Circularly Polarized Luminescence: The Success of d-Block and f-Block Chiral Complexes. *Front. Chem.* **2020**, *8* (July), 1−27.

(15) Richardson, F. S. Theory of Optical Activity in the Ligand-Field Transitions of Chiral Transition Metal Complexes. *Chem. Rev.* **1979**, *79* (1), 17−36.

(16) Kubo, H.; Shimizu, D.; Hirose, T.; Matsuda, K. Circularly Polarized Luminescence Designed from Molecular Orbitals: A Figure-Eight-Shaped [5]Helicene Dimer with D 2 Symmetry. *Org. Lett.* **2020**, *22*, 9276−9281.

(17) Sinha, N.; Yaltseva, P.; Wenger, O. S. The Nephelauxetic Effect Becomes an Important Design Factor for Photoactive First-Row Transition Metal Complexes. *Angew. Chem., Int. Ed.* **2023**, *62* (30), No. e202303864.

(18) Chong, J.; Besnard, C.; Cruz, C. M.; Piguet, C.; Jiménez, J. R. Heteroleptic Mer-[Cr(N∩N∩N)(CN)3] Complexes: Synthetic Challenge, Structural Characterization and Photophysical Properties. *Dalton Trans.* **2022**, *51* (11), 4297−4309.

(19) Reichenauer, F.; Zorn, D.; Naumann, R.; Förster, C.; Heinze, K. Factorizing the Nephelauxetic Effect in Heteroleptic Molecular Rubies. *Inorg. Chem.* **2024**, *63* (50), 23487−23496.

(20) Jiménez, J. R.; Poncet, M.; Doistau, B.; Besnard, C.; Piguet, C. Luminescent Polypyridyl Heteroleptic CrIIIcomplexes with High Quantum Yields and Long Excited State Lifetimes. *Dalton Trans.* **2020**, *49* (39), 13528−13532.

(21) Sawicka, N.; Craze, C. J.; Horton, P. N.; Coles, S. J.; Richards, E.; Pope, S. J. A. Long-Lived, near-IR Emission from Cr(III) under Ambient Conditions. *Chem. Commun.* **2022**, *58*, 5733.

(22) Jones, R. W.; Cowin, R. A.; Ivalo, I. I.; Chekulaev, D.; Roseveare, T. M.; Rice, C. R.; Weinstein, J. A.; Elliott, P. I. P.; Scattergood, P. A. A Near-Infrared Luminescent Cr(III) N-Heterocyclic Carbene Complex. *Inorg. Chem.* **2024**, *63* (19), 8526−8530.

(23) Ye, Y.; Poncet, M.; Yaltseva, P.; Salcedo Abraira, P.; Rodriguez Dieguez, A.; Martín, J. H.; Cuevas-Contreras, L.; Cruz, C. M.; Doistau, B.; Piguet, C.; Wenger, O. S.; et al. Modulating the Spin−Flip Rates and Emission Energies through Ligand Design in Chromium(III) Molecular Rubies. *Chem. Sci.* **2025**, *16*, 5205−5213.

(24) Rosenfeld, L. Quantenmechanische Theorie der natürlichen optischen Aktivität von Flüssigkeiten und Gasen. *Z. Phys.* **1929**, *52*, 161−174.

(25) Ziegler, M.; Von Zelewsky, A. Charge-Transfer Excited State Properties of Chiral Transition Metal Coordination Compounds Studied by Chiroptical Spectroscopy. *Coord. Chem. Rev.* **1998**, *177* (1), 257−300.

(26) Gendron, F.; Moore II, B.; Cador, O.; Pointillart, F.; Autschbach, J.; Le Guennic, B. Ab-Initio Study of Circular Dichroism and Circularly Polarized Luminescence of Spin-Allowed and Spin-Forbidden Transitions: From Organic Ketones to Lanthanide Complexes. *J. Chem. Theory Comput.* **2019**, *15*, 4140−4155.

(27) Dee, C.; Zinna, F.; Kitzmann, W. R.; Pescitelli, G.; Heinze, K.; Di Bari, L.; Seitz, M. Strong Circularly Polarized Luminescence of an Octahedral Chromium(III) Complex. *Chem. Commun.* **2019**, *55* (87), 13078−13081.

(28) Llunell, M.; Casanova, D.; Cirera, J.; And, P. A.; Alvarez, S. *Program for the Stereochemical Analysis of Molecular Fragments by Means of Continuous Shape Measures and Associated Tools, SHAPE*, Version 2.1; Universitat de Barcelona: Barcelona, Spain, 2013.

(29) Zare, D.; Doistau, B.; Nozary, H.; Besnard, C.; Guénée, L.; Suffren, Y.; Pelé, A. L.; Hauser, A.; Piguet, C. CrIII as an Alternative to RuII in Metallo-Supramolecular Chemistry. *Dalton Trans.* **2017**, *46* (28), 8992−9009.

(30) Förster, C.; Osthues, H.; Schwab, D.; Doltsinis, N. L.; Heinze, K. Quantum Chemical Study of the Pressure-Dependent Phosphorescence of [Cr(ddpd)2]3+ in the Solid State. *ChemPhysChem* **2023**, *24* (12), 1−7.

(31) Otto, S.; Harris, J. P.; Heinze, K.; Reber, C. Molecular Ruby under Pressure. *Angew. Chem., Int. Ed.* **2018**, *57* (34), 11069−11073.

(32) Juban, E. A.; McCusker, J. K. Ultrafast Dynamics of 2E State Formation in Cr(Acac)3. *J. Am. Chem. Soc.* **2005**, *127* (18), 6857−6865.

https://doi.org/10.1021/jacs.5c06196
J. Am. Chem. Soc. 2025, 147, 23827−23833

(33) Ferguson, J. Spectroscopy of 3d Complexes. *Prog. Inorg. Chem.* **1970**, *12*, 159−293.
(34) Sinha, N.; Jiménez, J. R.; Pfund, B.; Prescimone, A.; Piguet, C.; Wenger, O. S. A Near-Infrared-II Emissive Chromium(III) Complex. *Angew. Chem., Int. Ed.* **2021**, *60* (44), 23722−23728.
(35) Reichenauer, F.; Wang, C.; Förster, C.; Boden, P.; Ugur, N.; Báez-Cruz, R.; Kalmbach, J.; Carrella, L. M.; Rentschler, E.; Ramanan, C.; Niedner-schatteburg, G.; Gerhards, M.; Seitz, M.; Resch-genger, U.; Heinze, K. Strongly Red-Emissive Molecular Ruby [Cr(bpmp) 2] 3+ Surpasses [Ru(bpy) 3] 2+. *J. Am. Chem. Soc.* **2021**, *143*, 11843−11855.
(36) Witzke, H. Semi-Empirical Evaluations of the Racah B and C Parameters from the Crystal Field Spectra of Chromium(III) Complexes. *Theor. Chim. Acta* **1971**, *20* (2), 171−185.
(37) Yarranton, J. T.; McCusker, J. K. Ligand-Field Spectroscopy of Co(III) Complexes and the Development of a Spectrochemical Series for Low-Spin D6Charge-Transfer Chromophores. *J. Am. Chem. Soc.* **2022**, *144* (27), 12488−12500.
(38) Cheng, Y.; He, J.; Zou, W.; Chang, X.; Yang, Q.; Lu, W. Circularly Polarized Near-Infrared Phosphorescence of Chiral Chromium(Iii) Complexes. *Chem. Commun.* **2023**, *59* (13), 1781−1784.
(39) Tsurui, M.; Takizawa, R.; Kitagawa, Y.; Wang, M.; Kobayashi, M.; Taketsugu, T.; Hasegawa, Y. Chiral Tetrakis Eu(III) Complexes with Ammonium Cations for Improved Circularly Polarized Luminescence. *Angew. Chem., Int. Ed.* **2024**, *63* (34), No. e202405584.
(40) Hatanaka, M.; Yabushita, S. Theoretical Study on the F-f Transition Intensities of Lanthanide Trihalide Systems. *J. Phys. Chem. A* **2009**, *113* (45), 12615−12625.
(41) Nagata, Y.; Mori, T. Irreverent Nature of Dissymmetry Factor and Quantum Yield in Circularly Polarized Luminescence of Small Organic Molecules. *Front. Chem.* **2020**, *8* (June), 1−6.

https://doi.org/10.1021/jacs.5c06196
J. Am. Chem. Soc. 2025, 147, 23827−23833